Award Number: W81XWH-09-1-0609

TITLE: "Acquisition of High Field Nuclear Magnetic Resonance Spectrometers for Research in Molecular structure, Function and Dynamics"

PRINCIPAL INVESTIGATOR: George R. Pack

CONTRACTING ORGANIZATION: University of Louisville, Louisville, KY 40202

REPORT DATE: September 2012

TYPE OF REPORT: Final

PREPARED FOR: U.S. Army Medical Research and Materiel Command
Fort Detrick, Maryland 21702-5012

# REPORT DOCUMENTATION PAGE

*Form Approved*
*OMB No. 0704-0188*



| **1. REPORT DATE** | **2. REPORT TYPE** | **3. DATES COVERED** |
|---|---|---|
| September 2012 | Final | 10 August 2009- 09 August 2012 |

**4. TITLE AND SUBTITLE**
Acquisition of High Field Nuclear Magnetic Resonance Spectrometers for Research in Molecular structure, Function and Dynamics

**5a. CONTRACT NUMBER**

**5b. GRANT NUMBER**
W81XWH-09-1-0609

**5c. PROGRAM ELEMENT NUMBER**

**6. AUTHOR(S)**
George R. Pack
george.pack@louisville.edu

**5d. PROJECT NUMBER**

**5e. TASK NUMBER**

**5f. WORK UNIT NUMBER**

**7. PERFORMING ORGANIZATION NAME(S) AND ADDRESS(ES)**
University of Louisville, Louisville, KY 40202

**8. PERFORMING ORGANIZATION REPORT NUMBER**

**9. SPONSORING / MONITORING AGENCY NAME(S) AND ADDRESS(ES)**
U.S. Army Medical Research and Materiel Command
Fort Detrick, Maryland 21702-5012

**10. SPONSOR/MONITOR'S ACRONYM(S)**

**11. SPONSOR/MONITOR'S REPORT NUMBER(S)**

**12. DISTRIBUTION / AVAILABILITY STATEMENT**
Approved for Public Release; Distribution Unlimited

**13. SUPPLEMENTARY NOTES**

**14. ABSTRACT**

This work combines the work of four investigators in the Department of Chemistry at the University of Louisville. All of the projects require high-field NMR and other techniques of Structural Biology for their completion. Two high-field NMR spectrometers, one operating at 400 MHz and one at 700 MHz, were purchased installed and tested.

**15. SUBJECT TERMS**- none provided

| **16. SECURITY CLASSIFICATION OF:** | | | **17. LIMITATION OF ABSTRACT** | **18. NUMBER OF PAGES** | **19a. NAME OF RESPONSIBLE PERSON** |
|---|---|---|---|---|---|
| | | | | | USAMRMC |
| **a. REPORT** | **b. ABSTRACT** | **c. THIS PAGE** | | | **19b. TELEPHONE NUMBER** *(include area code)* |
| U | U | U | UU | 28 | |

## Table of Contents

**Introduction**

This work combines the work of four investigators in the Department of Chemistry at the University of Louisville. All of the projects require high-field NMR and other techniques of Structural Biology for their completion. Two high-field NMR spectrometers, one operating at 400 MHz and one at 700 MHz, were purchased installed and tested. The projects have all achieved their basic goals and resulted in eighteen publications, which are included as an Appendix.

The four projects are:

a. Mechanism of conversion of uridine to pseudouridine and to 4-thiouridine (Dr. E. G. Mueller).
b. Devising new nanocomposites that can enhance wound healing (Dr. M. C. Yappert).
c. Characterization of the complex between Factor XIII and fibrinogen (Dr. M. C. Maurer).
d. Tensile properties of fibrous proteins (Dr. R. J. Wittebort)

These will each be described independently, below.

**Task 1. Mechanism of conversion of uridine to pseudouridine and to 4-thiouridine (Dr. E. G. Mueller).**

RNA containing 5-fluorouridine (F(5)U) had previously been used to examine the mechanism of the pseudouridine synthase TruA, formerly known as pseudouridine synthase I [Gu et al. (1999) Proc. Natl. Acad. Sci. U.S.A. 96, 14270-14275]. From that work, it was reasonably concluded that the pseudouridine synthases proceed via a mechanism involving a Michael addition by an active site aspartic acid residue to the pyrimidine ring of uridine or F(5)U. Those conclusions rested on the assumption that the hydrate of F(5)U was obtained after digestion of the product RNA and that hydration resulted from hydrolysis of the ester intermediate between the aspartic acid residue and F(5)U. As reported here, (18)O labeling definitively demonstrates that ester hydrolysis does not give rise to the observed hydrated product and that digestion generates not the expected mononucleoside product but rather a dinucleotide between a hydrated isomer of F(5)U and the following nucleoside in RNA. The discovery that digestion products are dinucleotides accounts for the previously puzzling differences in the isolated products obtained following the action of the pseudouridine synthases TruB and RluA on F(5)U in RNA.

The reference for this work, included in the Appendix, is:

McDomald, MK, Miracco, EJ, Chen JJ, Xie YZ and Mueller, EG "The Handling of the Mechanistic Probe 5-Fluorouridine by the Pseudouridine Synthase TruA and Its Consistency with the Handling of the Same Probe by the Pseudouridine Synthases TruB and RluA" Biochemistry **50**, 426-436, 2011.

The pseudouridine synthase TruB handles 5-fluorouridine in RNA as a substrate, converting it into two isomeric hydrated products. Unexpectedly, the two products differ not in the hydrated pyrimidine ring but in the pentose ring, which is epimerized to arabinose in the minor product. This inversion of stereochemistry at C2′ suggests that pseudouridine generation may proceed by a mechanism involving a glycal intermediate or that the previously proposed mechanism involving an acylal intermediate operates but with an added reaction manifold for 5-fluorouridine versus uridine. The arabino product strongly disfavors a mechanism involving a Michael addition to the pyrimidine ring.

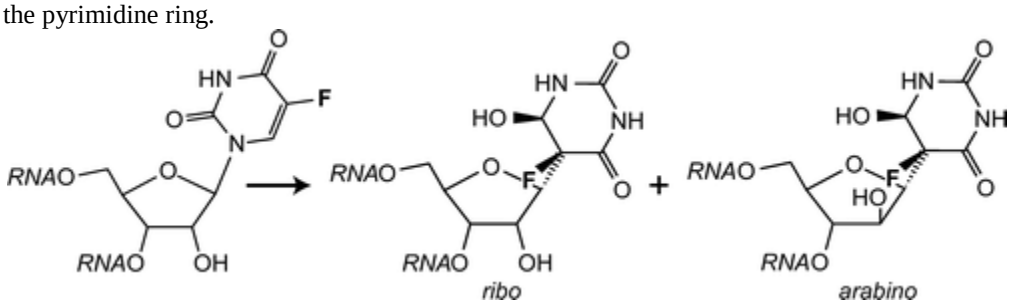


This was published as a JACS Communication.

The reference for this work, which is included in the Appendix, is:

> Miracco, EJ and Mueller, EG "The Products of 5-Fluorouridine by the Action of the Pseudouridine Synthase TruB Disfavor One Mechanism and Suggest Another" J. Amer. Chem. Soc. 133, 1826–118292011, 2011.

As part of the investigation of the pseudouridine synthases, 5-fluorouridine in RNA was employed as a mechanistic probe. The hydrated, rearranged product of 5-fluorouridine was isolated as part of a dinucleotide and found to undergo unusual fragmentation during mass spectrometry, with the facile loss of HNCO from the product pyrimidine ring favored over phosphodiester bond rupture. Although the loss of HNCO from uridine and pseudouridine is well established, the pericyclic process leading to their fragmentation cannot operate with the saturated pyrimidine ring in the product of 5-fluorouridine. Based on the MS(n) results and calculations reported here, a new mechanism relying on the peculiar disposition of the functional groups of the product pyrimidine ring was proposed to account for the unusually facile fragmentation.

The reference for this work, included in the Appendix, is:

Miracco, EJ, Bogdanov, B and Mueller, EG "Unexpected linear ion trap collision-induced dissociation and Fourier transform ion cyclotron resonance infrared multi-photon dissociation fragmentation of a hydrated *C*-glycoside of 5-fluorouridine formed by the action of the pseudouridine synthases RluA and TruB" *Rapid Comm. Mass Spect*. 25, 2627-2632 (2011).

**Task 2. Devising new nanocomposites that can enhance wound healing (Dr. M. C. Yappert).**

1) *Confirmation and correction the assignments of $^{1}H$ NMR resonances of sodium cholate (NaCho) primary and secondary micelles:* The high resolution and sensitivity of the 700 MHz instrument enabled the correction of mis-assignments of resonances in spectra originally acquired with the 500 MHz instrument. Fortunately, this error did not affect the 'barrel' model proposed for the primary micelles (as included in the reports submitted last year). Furthermore, the through-space interactions obtained from the Rotating Frame Overhauser Effect Spectroscopy (ROESY) experiments acquired with the new instrument showed relevant off-diagonal peaks that support the 'barrel' model. All figures and tables have been revised and will be submitted for publication shortly.

2) *Interactions between fatty acids and NaCho micelles:* Although several models have been proposed for the molecular arrangement of NaCho micelles, little is known about their interactions with fatty acids. In this study, the interactions of two fatty acids, oleic acid (OA, 18:1) and stearic acid (SA, 18:0) with NaCho were investigated. Our hypothesis was that because the site of unsaturation causes OA to be in the liquid crystalline phase, this fatty acid would be inserted into the hydrophobic core of the previously proposed 'barrel-like' primary micelles model. Conversely, SA is in its gel phase and was predicted not to interact with the micelles due to rigidity of the saturated tail. This postulate was tested using 1D and 2D NMR experiments carried out with the 700 MHz NMR instrument. The results from ROESY experiments confirmed that OA interacts with NaCho but SA does not. However, OA does not enter the hydrophobic core of the primary micelles. Key through-space interactions revealed by the ROESY spectra, suggest that OA "drapes" around the exterior of the micelle and leads to the aggregation of neighboring micelles also draped with OA. A "brick and mortar" model is postulated for the mixed micellar arrangement. The undergraduate student involved in these studies, Katherine Dormeney, presented a poster at the end of the Research Summer program, on August 1, 2012.

**Task 3. Characterization of the complex between Factor XIII and fibrinogen (Dr. M. C. Maurer).**

Members of the coagulation cascade have far reaching effects on stemming blood loss, promoting wound healing, and controlling heart disease, stroke, and arteriosclerosis. In the clotting process, thrombin cleaves off the N-terminal portions of the Aα and Bβ chains of fibrinogen $(A\alpha B\beta\gamma)_2$ to release FpA and FpB (1). The resultant fibrin monomers polymerize into ordered fibrin arrays that are later cross-linked by Factor XIII (FXIII) (2). In addition to cleaving fibrinogen, thrombin is also involved in activating FXIII and initiating platelet activation by cleaving the protease activated receptors (PARs) (3). The main objective of this research has been to characterize the structural and kinetic properties of proteins that contribute to forming a stronger blood clot. Knowledge gained may aid in the design of innovative new therapeutic agents.

Project 1 Activated Factor XIII (FXIII) is a transglutaminase that is responsible for catalyzing the formation of γ-glutamyl-ε-lysyl crosslinks within a fibrin blood clot network (2). One of the binding sites for FXIII on fibrin has been found within αC 242-424, a segment located in the C-terminal portion of the fibrinogen Aα chain(4). A key research goal has been to examine the structural and dynamic properties that govern interactions between FXIII and Fbg αC 242-424.

An *E. coli* expression system for αC (233-425) has been successfully established in the laboratory (5). Protein has been expressed and purified from standard media and also from minimal media used to produce $^{15}N$ labeled material. The first $^{15}N$-HSQC spectra for $^{15}N$- αC (233 – 425) were attained on the 700 MHz Varian NMR equipped with a triple resonance cryoprobe and

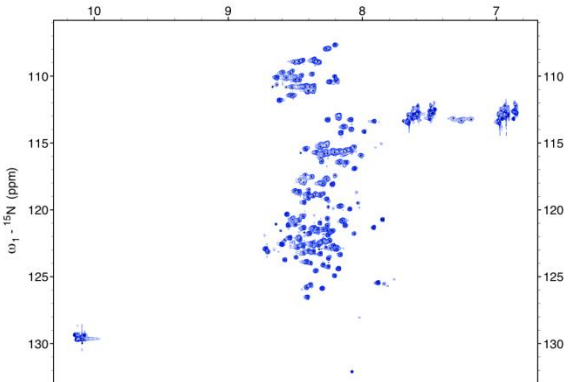


$^{15}N$-HSQC of $^{15}N$- αC (233 – 425) at 20ºC

confirmed on the 800 MHz Varian NMR. This 2D NMR experiment monitors the protons ($^{1}H$) attached to any $^{15}N$ labeled amino acid groups. The NMR sample contained 210 µM αC (233 – 425) in PBS buffer at pH 6.6. The αC (233 – 425) $^{15}N$-HSQC reported on 184 of the 199 possible $^{1}H$ signals. The narrow $^{1}H$ crosspeak dispersion within the 8-9 ppm range suggests that αC (233 – 425) is an intrinsically disordered protein. There is great interest in knowing whether further structure will be adopted upon binding to cellular FXIII $A_2$ and/or plasma FXIII $A_2B_2$. Mutation studies already predict regions of αC (233 – 425) that bind to FXIII (5).

Project 2 Besides assessing structural features, we have also been implementing assays for following the reactivity of FXIII toward glutamine-containing substrates. Both NMR and mass spectrometry approaches has been employed. In preparation for future studies with αC (233 – 425), we have been optimizing NMR methods to monitor transglutaminase reactions on a series of glutamine-containing substrate peptides with $^{15}NH_4Cl$ serving as a mimic for the lysine-containing substrate (6). Activated FXIII catalyzes the exchange of the $^{14}NH_2$ on substrate glutamine side chains for the $^{15}NH_2$ on the $NH_4Cl$. This kind of exchange can be detected by 1D and 2D $^{15}N$-HSQC experiments (6)

FXIII catalyzed reactions revealed that the $^{15}NH_2$ from $^{15}NH_4Cl$ could indeed be incorporated into the reactive glutamines of the substrate peptides $\alpha_2$AP (1-15) Q4P and TAFI (1-15). These peptides are derived from proteins involved in regulating degradation of fibrin clots. Below is a sample 2D $^{15}N$-HSQC spectrum collected on the 700 MHz NMR for $\alpha_2$AP (1-15) Q4P. The glutamines undergoing the $^{15}N$ labeled transformation showed the presence of two amide proton side chains in the 6-7.4 ppm region. These protons were attached to a $^{15}N$ group that is observed at approximately 112 ppm.

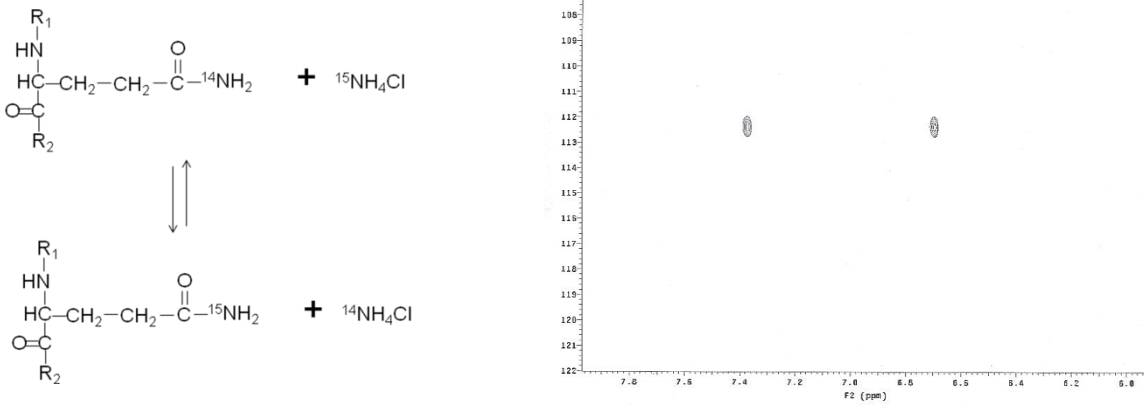


Following the Reactivity of Glutamine-Containing FXIII Reactions- The left panel shows the isotopic reaction being followed. The right panel is a 2D $^{15}N$-HSQC spectrum for a reaction involving 400 nM FXIIIa + 200 µM $\alpha_2$AP Q4P (1-15) + $^{15}NH_4Cl$ in 50 mM $CaCl_2$ and 20 mM Borate, pH 7.4.

The contributions of individual substrate amino acids in controlling FXIIIa transglutaminase activity is not well understood. Unlike the coupled uv-vis assays of the past (7-9), we have been using a MALDI-TOF mass spectrometry assay that we developed. Activated FXIII catalyzes the cross-linking between a Q-containing peptide and glycine-ethylester (GEE). The reactions are quenched at distinct time points using EDTA. MALDI mass spectra are then used to detect the consumption of free peptide and production of cross-linked peptide-GEE. FXIIIa substrate sequences related to $\alpha_2$-antiplasmin ($\alpha_2$AP), *S. Aureus* fibronectin binding A (FbnA), and thrombin-activatable fibrinolysis inhibitor (TAFI) have been examined. The kinetic studies reveal that residues surrounding the reactive glutamines and at a more distant position promote productive anchoring on to the FXIII active site surface. This MALDI based MS assay has been tested to study the kinetics associated with the binding of FXIII to αC (233-425). This fibrinogen domain contains three reactive glutamines (Qs).

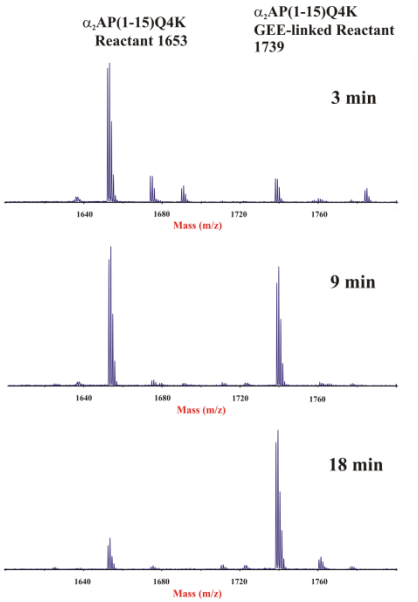

Introducing a chymotrypsin proteolytic step after the kinetic quench has made it possible to use MALDI to monitor crosslinking of GEE to the FXIII reactive αC Q328. Strategies to probe the other glutamines are ongoing. A manuscript on the original MALDI-MS assay design is in preparation.

Project 3 Understanding how specific FXIII and thrombin residues participate in binding and regulating hydrolysis may lead to the design of FXIII enzymes whose degree of activation and optimal target site can be controlled. Knowledge gained may also lead to the production of clotting environments with distinct characteristics. An important focus has been on examining the HPLC based kinetics associated with hydrolysis of FXIII activation peptides (APs) at the R37-G38 peptide bond by the recombinant anticoagulant thrombin mutants W215A, E217A, W215A/E217A, W60dA, and Y60aA. FXIII AP (28-41) peptides have contained V34X substitutions including L34, P34 and F34. The thrombin mutants respond differently depending upon which of these $P_4$ residues (V34X) is present in the substrate activation peptide

Following FXIII Kinetics by MALDI- MS

FXIII AP P34 resembles the protease activated receptor PAR4 whereas F34 exhibits the same thrombin-bound $P_4$ to $P_2$ NMR interactions (10) as observed with the cardioprotective FXIII AP L34 (11). FXIII activation peptides containing V34, L34, or P34 could each be accommodated by alanine mutants of thrombin lacking either the W60d or Y60a residue of the 60-insertion loop. By contrast, FXIII F34 AP could be cleaved by thrombin W60dA but not by Y60aA. FXIII P34 is highly reliant on the thrombin W215 platform for its strong substrate properties whereas FXIII F34 AP becomes the first segment that can maintain its $K_m$ upon loss of the critical thrombin W215 residue. Interestingly, FXIII F34 AP could also be readily accommodated by thrombin L99A and E217A. Hydrolysis of FXIII F34 AP by thrombin W217A/E217A (WE) was similar to that of FXIII L34 AP whereas WE could not effectively cleave FXIII P34 AP. FXIII F34 and P34 AP thus show much promise for designing FXIII activation systems that are either tolerant of or greatly hindered by the presence of anticoagulant thrombins. These kinetic studies were published in 2011 (12).

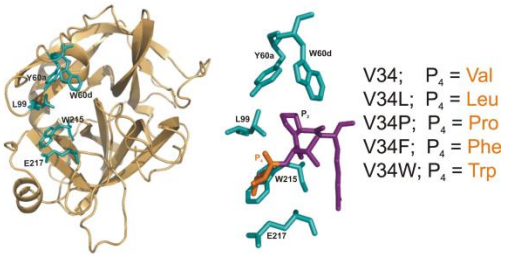


Thrombin (Tan, Cyan) + AP 33-37 (Orange and Purple). Individual mutants are highlighted.

As found with FXIII F34 AP (10), the peptides FXIII W34 AP, fibrinopeptide B (5-18), and PAR3 (44-56) all contain aromatic residues. 1D proton line broadening and 2D transferred NOESY projects have been carried out on the three new thrombin-peptide complexes using the 700 MHz NMR. The results obtained demonstrate the importance of such aromatic residues in promoting binding interactions with thrombin. Efforts in this research area are ongoing.

Project 4 NMR studies can be very effective for examining structural features, mapping sites of contact for enzyme-ligand complexes, and assessing protein dynamics. Amide proton hydrogen-deuterium exchange (HDX) coupled with MALDI-TOF mass spectrometry (MS) is a complementary method for probing large and challenging systems. Moreover, HDX-MS can examine protein regions where NMR chemical shifts cannot be assigned (13). FXIII $A_2$ is quite large in size for NMR and thrombin is highly dynamic. Both protein systems are thus ideal for the complementary HDX approach.

Comparing FXIII $A_2$ and the A monomer

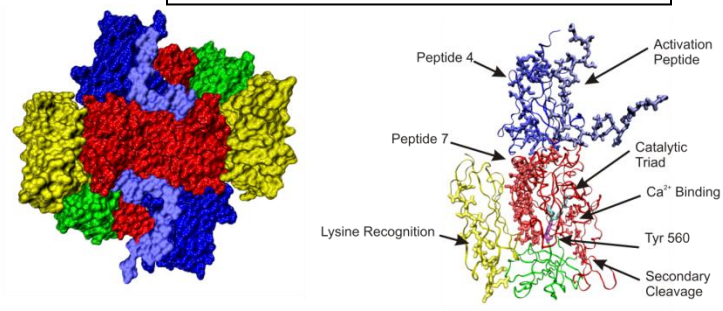


FXIII $A_2$ can be activated proteolytically with thrombin and low mM $Ca^{2+}$ or nonproteolytically with high monovalent/divalent cations along with low mM $Ca^{2+}$. Physiologically, FXIII $A_2$ is poised to respond to transient influxes of $Ca^{2+}$ in a $Na^+$ containing environment (14). FXIII $A_2$ was examined by HDX-MS approaches in the presence of different cations ($Ca^{2+}$, $Mg^{2+}$, $Ba^{2+}$, $Cu^{2+}$, $Na^+$) ranging from 1-2 mM, physiological $Ca^{2+}$ concentration, to 50-500mM for nonproteolytic activation. Increases in FXIII solvent exposure could already be observed at 1 mM $Ca^{2+}$ for the dimer interface, the catalytic

site, and glutamine substrate regions. By contrast, solvent protection was observed at the secondary cleavage site. These events occurred even though 1mM $Ca^{2+}$ is insufficient for FXIII activation. The metals 1mM $Mg^{2+}$, 1mM $Ba^{2+}$, and 1mM $Cu^{2+}$ each led to conformational changes, many in the same FXIII regions as $Ca^{2+}$. These different HDX studies help reveal the first FXIII segments that respond to physiological $Ca^{2+}$ levels. A manuscript on this project was published in 2011 (15).

Thrombin participates in coagulation, anticoagulation, and initiation of platelet activation. To fulfill its diverse roles and maintain hemostasis, this serine protease is regulated via the extended active site region and anion binding exosites I and II (ABE I and ABE II) (16). Some agents that target thrombin ABE-I include fibrin(ogen), hirudin, PAR1, PAR3, and thrombomodulin. By contrast, heparin, fibrinogen γ', FVIII, and GpIbα bind thrombin ABE-II. Interestingly, fibrin binding to ABE-I aids in promoting thrombin activation of plasma FXIII $A_2B_2$ (17). HDX-MS has been used to characterize ligand binding to individual thrombin exosites and to investigate the presence of exosite-active site and exosite-exosite interactions. The protease activated receptors ligands PAR3 (44-56) and PAR1 (49-62) were observed to bind to thrombin ABE I and then to exhibit long range effects over to ABE II. By contrast, the leech anticoagulant Hirudin (54-65) focused more on ABE I and did not transmit influences over to ABE II (18). Although these three ligands were each directed to ABE I, they did not promote the same conformational consequences. PPACK inhibition at the thrombin active site led to further local and long range consequences to thrombin-ABE I ligand complexes with the autolysis loop often most affected. When Hirudin (54-65) was bound to ABE I, it was still possible to bind GpIbα (269-286) or fibrinogen γ' (410-427) to ABE II. Each ligand exerted its predominant influences on thrombin and also allowed inter-exosite communication. The results obtained support the proposal that thrombin is a highly dynamic protein. The transmission of ligand-specific local and long range conformational events is proposed to help regulate this multi-functional enzyme. A manuscript on this project was just submitted.

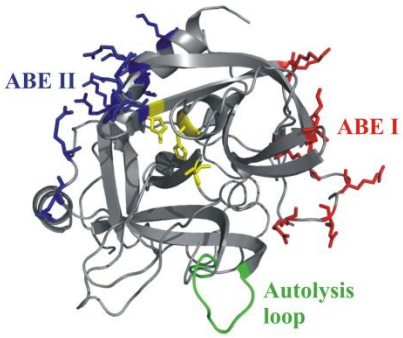


Thrombin structure highlighting the active site (yellow), anion binding exosite II (blue), anion binding exosite I (red), and autolysis loop (green).

**Task 4. Tensile properties of fibrous proteins (Dr. R. J. Wittebort)**

Comparisons between rubber and elastin for the amount of stretch induced changes in ordered solvent and the degree of ordering, clearly indicate important differences in their elastic mechanisms. The increase of the amount of ordered solvent with approximately constant quadrupolar coupling upon stretch are distinct from the results for rubber and indicate a significant role of the solvent in the elastic mechanism of elastin. Moreover, the increase in solvent ordering with increased temperature, demonstrates the importance of the hydrophobic effect in elastin recoil. From this perspective we studied the variations in the amount of ordered solvent and strength of recoil when the hydrophobicity of the polymer is systematically varied. These studies used designed elasrin-like sequences prepared using recombinant protein methods.

Efficient and versatile computer algorithms were developed for quantum mechanical simulation of spin-1 ($^2H$) and spin-5/2 ($^{17}O$) NMR experiments. The code incorporates coherent evolution and relaxation of the spin density operator. New and practical double quantum $^2H$ NMR experiments for quantitative determination of the amount of ordered water and the degree of water ordering as a function of temperature, mechanical stretch and water activity were developed.

We have found a 10-fold increase in the amount of ordered water when fibers are maximally stretched (150% of resting length). Water ordering, however, remains approximately constant, i.e. is similar to relaxed fibers.
We then modified a probe to determine the anisotropy of the ordering relative to the stretch axis and compared results for the hydrate of elastin with latex rubber swollen in an organic solvent, deuterochloroform. Unlike elastin, only the degree of solvent ordering is affected. Stretch-induced ordering of the rubber matrix orders the solvent but does not change the fraction of solvent interacting with the rubber matrix. *A fundamental difference in the interaction of water with elastin (a hydrophobic protein) and a hydrophobic solvent interacting with latex rubber*

*(also hydrophobic) is observed.* Elastin stretch increases the hydrophobic surface that contacts water. With a statistical mechanical model, the spectroscopic results indicate that stretch induced water ordering makes a significant contribution to elastin's recoil force.

Based on the above, we are designing synthetic protein elastomers with tunable properties. The initial design was recently expressed by our collaborator at City College, NYC.

Key Research Accomplishments

**Task 1. Mechanism of conversion of uridine to pseudouridine and to 4-thiouridine (Dr. E. G. Mueller).**
* The previously accepted mechanism of pseudouridine synthase TruA was shown to be incorrect. Instead of the expected product, the hydration product was demonstrated to be a dinucleodide. (McDonald et al, 2011)
* TruB, which handles the mechanistic probe 5-fluoroidine in RNA as a simple substrate rather than making a tight adduct (as Tru A does), converts 5-FU into two isomeric hydrated products that differ not in the hydrated pyrimidine ring but in the pentose ring, which is epimerized to arabinose in the minor product. This finding immediately suggested *a new mechanism* involving a glycal intermediate for the isomerization of uridine to pseudouridine. (Miracco and Mueller, 2011)
* The hydrated, rearranged product of 5-fluorodine, isolated as part of a dinucleoside, was found to undergo an unusual fragmentation during Mass spectrometry, with facile loss of HNCO from the product pyrimiding ring favored over phosphodiester bond rupture. Because the pericyclic process leading to this fragmentation cannot operate on a saturated pyrimidine ring, *a new mechanism was proposed*, which relies on the peculiar disposition of the functional groups of the product pyrimidine ring. (Miracco et al, 2011)

T**ask 2. Devising new nanocomposites that can enhance wound healing (Dr. M. C. Yappert).**
** Confirmation and correction the assignments of $^{1}H$ NMR resonances of sodium cholate (NaCho) primary and secondary micelles:* The high resolution and sensitivity of the 700 MHz instrument enabled the correction of mis-assignments of resonances in spectra originally acquired with the 500 MHz instrument. Fortunately, this error did not affect the 'barrel' model proposed for the primary micelles (as included in the reports submitted last year). Furthermore, the through-space interactions obtained from the Rotating Frame Overhauser Effect Spectroscopy (ROESY) experiments acquired with the new instrument showed relevant off-diagonal peaks that support the 'barrel' model. All figures and tables have been revised and will be submitted for publication shortly.

**a)** * *Interactions between fatty acids and NaCho micelles:* **Interactions between hyaluronan and lipids.** The hypothesis is that the age-dependent liquefaction of the vitreous humor in human eyes is the result of the interaction of lipid metabolites derived from the lens and retina. These interactions are expected to disrupt hyaluronan/collagen/water interactions and cause liquefaction of the vitreous gel. Our results indicate that the higher concentration of lipid metabolites is the posterior region of the vitreous humor, near the retina. Model studies were carried out with hyaluronan and lipids with different chain lengths and degree of unsaturation.

*1)* Two very powerful two-dimensional NMR experiments, Heteronuclear Single Quantum Correlation (HSQC) and Heteronuclear Multiple Bond Correlation (HMBC) were also applied to hyaluronic acid disaccharide sodium salt or alpha-4-deoxy-L-*threo*-hex-4-enopyranosyluronic acid-[1→3] (α-ΔGlcU-(1→3)-GlcNAc or ΔDiHA). Importantly, mutorotation led to the presence of not just the alpha anomer, but also the beta anomer. The new instrument enabled the complete assignment of all resonances in the sample containing the two anomers. This is a significant accomplishment. In addition, the interactions of the ΔDiHA with 1-oleoyl-2-hydroxy-*sn*-glycero-3-phosphocholine (LPC-OA), 1,2-dipalmitoyl-*sn*-glycerol (DAG), stearic acid (SA) and oleic acid (OA) were studied. The graduate student involved in these studies, Kristen Magness, defended her Ph.D. degree on July 11, 2012.

*2)* The polymeric form of HA was then investigated in $D_2O$ and its interactions with various lipids were probed. The analysis of chemical shifts and bandwidths of $^{1}H$ NMR resonances revealed the strongest interactions to be between HA and unsaturated oleic acid and lyso-oleoyl-phosphatidylcholine.

**Task 3. Characterization of the complex between Factor XIII and fibrinogen (Dr. M. C. Maurer).**
* An *E. coli* expression system for fibrinogen αC (233-425) was successfully established in the laboratory. The first $^{15}N$-HSQC spectra for $^{15}N$- αC (233 – 425) were attained on the 700 MHz Varian NMR equipped with a triple

resonance cryoprobe and confirmed on the Brown Cancer Center 800 MHz Varian NMR. Results suggest this fragment is intrinsically disordered and may gain additional structure in the presence of Factor XIII (FXIII).
* NMR and MALDI-TOF mass spectrometry assays were developed for exploring the substrate specificity of Factor XIII. For the NMR based projects, 1D and 2D $^{15}$N-HSQC experiments were carried out. Activated FXIII could cross-link the $^{15}NH_2$ from $^{15}NH_4Cl$ into the reactive glutamines of substrate peptides based on $\alpha_2$AP (1-15) and TAFI (1-15). A new MALDI-TOF mass spectrometry assay was designed to directly follow the enzyme kinetics associated with the glutamine containing substrate. Amino acid positions in the vicinity of the reactive glutamine participate in promoting binding interactions with the FXIII active site surface.
* Kinetic and structural features that define interactions between peptide ligands and thrombin were elucidated. HPLC assays, 1D proton line broadening NMR, and/or 2D transferred NOESY NMR methods were used. The FXIII activation peptide segment 28-41 V34X targets the thrombin active site region whereas the PAR3 segment (44-56) binds to thrombin anion binding exosite I. Such interactions contribute to fibrin clot architecture and platelet activation.
* Hydrogen-Deuterium exchange coupled with MALDI-TOF mass spectrometry was used to probe conformational changes occurring to FXIII $A_2$, map FXIII $A_2B_2$ interactions, and characterize ligand binding to thrombin exosites. The roles that different divalent cations play in promoting activation of FXIII $A_2$ were assessed. Mapping studies revealed that the regulatory FXIII $B_2$ binds to catalytic FXIII $A_2$ along the $A_2$ dimer interface and $A_2$ β-barrels 1 and 2. Finally, ligands that target thrombin exosites were found to promote both local and long range conformational effects. Such events help regulate the multi-functional roles of thrombin.

**Task 4. Tensile properties of fibrous proteins (Dr. R. J. Wittebort)**
* New and practical double quantum $^2$H NMR experiments for quantitative determination of the amount of ordered water and the degree of water ordering as a function of temperature, mechanical stretch and water activity were developed.
* We find a 10-fold increase in the amount of ordered water when fibers are maximally stretched (150% of resting length). Water ordering, however, remains approximately constant, i.e. is similar to relaxed fibers.
* Elastin stretch increases the hydrophobic surface that contacts water. With a statistical mechanical model, the spectroscopic results indicate that stretch induced water ordering makes a significant contribution to elastin's recoil force.
* Based on the above, we are designing synthetic protein elastomers with tunable properties. The initial design was recently expressed by our collaborator at City College, NYC.

**Published Refereed Scientific Articles*:**

McDonald, MK, Miracco, EJ, Chen JJ, Xie YZ and Mueller, EG "The Handling of the Mechanistic Probe 5-Fluorouridine by the Pseudouridine Synthase TruA and Its Consistency with the Handling of the Same Probe by the Pseudouridine Synthases TruB and RluA" Biochemistry **50**, 426-436, (2011).

Miracco, EJ and Mueller, EG "The Products of 5-Fluorouridine by the Action of the Pseudouridine Synthase TruB Disfavor One Mechanism and Suggest Another" J. Amer. Chem. Soc. 133, 1826–118292011, (2011).

Miracco, EJ, Bogdanov, B and Mueller, EG "Unexpected linear ion trap collision-induced dissociation and Fourier transform ion cyclotron resonance infrared multi-photon dissociation fragmentation of a hydrated *C*-glycoside of 5-fluorouridine formed by the action of the pseudouridine synthases RluA and TruB". *Rapid Comm. Mass Spect*. 25, 2627-2632 (2011).

Maurer, M. C. "Liberating R169 promotes anticoagulant protein" *Blood* **120,** 501-502 (2012).

Jadhav, M.A., Lucas, R. C, Goldsberry, W. N. and Maurer, M.C. "Design of Factor XIII V34X activation peptides to control ability to interact with thrombin mutants." *Biochim Biophys. Acta - Proteins and Proteomics* **1814,** 1955-1963 (2011).

Woofter, R. T. and Maurer, Muriel C. "Role of calcium in the conformational dynamics of factor XIII activation examined by hydrogen-deuterium exchange coupled with MALDI-TOF MS." *Arch Biochem. Biophys*. **512,** 87-95 (2011).

Maurer, M. C. "Switching cation-binding loops paves the way for redesigning allosteric activation" *Proc. Natl. Acad. Sci USA* **108,** 5145-5146 (2011).

Jadhav, M. A.; Isetti, G, Trumbo, T. A. and Maurer, M.C. "Effects of Introducing Fibrinogen A alpha Character into the Factor XIII Activation Peptide Segment" *Biochemistry* 49, 2918-2924 (2010).

Sabo, T. M., Maurer, M. C. "Biophysical Investigation of GpIb alpha Binding to Thrombin Anion Binding Exosite II" *Biochemistry* 48, 7110-7122 (2009).

Faheem, S., Kim, S.-H., Nguyen, J., Neravetla, S., Ball, M., Foulks, G. N.,Yappert, M.C., Borchman, D. "Wax-tear and meibum protein, wax-beta-carotene interactions in vitro using infrared spectroscopy" *Exp'tl Eye Res*. **100,** 32-39 (2012).

Borchman, D., Foulks, G.N., Yappert, M.C. Milliner, SE "Differences in Human Meibum Lipid Composition with Meibomian Gland Dysfunction Using NMR and Principal Component Analysis" *Invest. Ophthal. Vis. Sci.* **53,** 337-347 (2012).

Borchman, D., Foulks, G.N., Yappert, M.C. Milliner, SE "Changes in Human Meibum Lipid Composition with Age Using Nuclear Magnetic Resonance Spectroscopy " *Invest. Ophthal. Vis. Sci.* **53,** 475-482 (2012).

Shrestha, R.K., Borchman, D. Foulks, G.N., Yappert, M.C., Milliner, S.E., "Analysis of the Composition of Lipid in Human Meibum from Normal Infants, Children, Adolescents, Adults, and Adults with Meibomian Gland Dysfunction Using (1)H-NMR Spectroscopy " *Invest. Ophthal. Vis. Sci.* **52,** 7350-7358 (2011).

Borchman, D., Foulks, G.N., Yappert, M.C., Bell, J., Wells, E., Neravetla, S., Greenstone, V. "Human Meibum Lipid Conformation and Thermodynamic Changes with Meibomian-Gland Dysfunction "" *Invest. Ophthal. Vis. Sci.* **52,** 3805-3817 (2011).

Borchman, D., Foulks, G. N., Yappert, M.C. "Confirmation of Changes in Human Meibum Lipid Infrared Spectra with Age Using Principal Component Analysis" *Current Eye Res*. **35,**778-786 (2010).

Borchman, D. and Yappert, M.C. "Lipids and the ocular lens" *J. Lipid Res*. **51,** 2473-2488 (2010).

Borchman, D., Yappert, M.C. and Foulks, G.N. "Changes in human meibum lipid with meibomian gland dysfunction using principal component analysis" *Exper. Eye Res.* **91**, 246-256 ( 2010).

Estrada, R., Puppato, A., Borchman, D., Yappert, M.C. "Reevaluation of the phospholipid composition in membranes of adult human lenses by P-31 NMR and MALDI MS" *Biochim. Biophys. Acta - Biomembranes* 1798, 303-311 (2010).

Borchman, D., Foulks, G.N., Yappert, M.C., Kakar, S., Podoll, N., Rychwalski, P., Schwietz, E. "Physical Changes in Human Meibum with Age as Measured by Infrared Spectroscopy" *Ophthal. Res.* **44,** 34-42 (2010).

Phillips, S.C., Triola, G., Fabrias, G., Goni, F.M., DuPre, D.B., Yappert, M.C. "cis- versus trans-Ceramides: Effects of the Double Bond on Conformation and H-Bonding Interactions" J. Phys. Chem B 113, 15249-15255 (2009).

Nyunt, M.T., Dicus, C.W., Cui, Y.-Y., Yappert, M.C., Huser, T.R., Nantz, M.H., Wu, J "Physico-Chemical Characterization of Polylipid Nanoparticles for Gene Delivery to the Liver" *Bioconj. Chem.* **20,** 2047-2054 (2009).

Lorkiewicz, P. and Yappert, M.C. Titania Microparticles and Nanoparticles as Matrixes for in Vitro and in Situ Analysis of Small Molecules by MALDI-MS" *Anal. Chem.* **81**, 6596-6603 (2009).

Pack, G.R. "Vital Molecules" editorial in *Thermodynamics and Catalysis* 3, 3-4, (2012).
*note: all publications from the laboratories of Professors Mueller, Maurer, Pack, Yappert and Wittbort for the time period of support are included.

**Students Supported**

Graduate Committee Chair: Professor Muriel Maurer

Doiphode, Prakash 7/1/2011 - 7/31/2011

Graduate Committee Chair: Professor Richard Wittebort

Krivokhizhina, Tatiana 8/1/2011 - 10/31/2011

**Degrees Awarded**

Graduate Committee Chair: Professor Eugene Mueller

Edd Miracco Ph.D. (awarded by the University of Delaware, work done at U of L, with equipment purchased with funds from this award) June 2011

Graduate Committee Chair: Professor Muriel Maurer

Madhavi Jadhav, Ph.D. 12/13/2011
Ricky Woofter, Ph.D. 12/13/2011
Prakash Doiphode, Ph.D. 12/13/2011

Graduate Committee Chair: Professor M. Cecilia Yappert

Shay Phillips, M.S. 2008; Ph.D. 12/15/2009
Kristen Magness, M.S. 2010; Ph.D. July, 2012. Degree to be awarded Dec. 2012
Sarah Milliner, M.S. 2012; Ph.D. expected 2013.

Graduate Committee Chair: Professor Richard Wittebort

Tatiana Krivokhizhina, Ph.D. 05/12/2012

**Employment or research opportunities applied for and/or received based on experience/training supported by this award**

Dr. Shay Phillips is Phillips is a group leader at Mead Johnson Nutrition in Evansville, IN.

Dr. Kristen Magniss will be a Chemistry professor at either Indiana University Southeast or Bellarmine College.

Dr. Madhavi A. Jadhav
Scientist I

Scientific Technical Services (Validation and Production)
Teva Pharmaceuticals
Forest, VA 24551

Ricky Woofter, PhD
Research Chemist, Bioanalytical Chemistry
WIL Research Laboratories, LLC
1407 George Rd.
Ashland, OH 44805

Edd Miracco
Post-doctoral fellow (Prof. Juli Feigon)
Department of Biochemistry
UCLA

Proposals Submitted:

**M. C. Yappert "A new technique for skin and soft tissue regeneration"** In collaboration with Dr. Sufan Chien of the Department of Surgery, this project involves the delivery of ATP to wounded tissue. A proposal was submitted on July 11, 2012 to the Department of the Army. The potential impact of this work is listed below (as written in the technical abstract of the proposal. "This is the first time a non-traditional approach is used to treat massive soft tissue defects. The success of this technique will overturn current paradigm in massive soft tissue defect—no surgery (except hemostasis and debridement), no tissue engineering, no transplantation, and no sacrifice of healthy body parts are required. It will significantly improve soldiers' post-traumatic life, save billions of dollars in healthcare costs, and has the potential to open up a new avenue for tissue regeneration applicable not only in acute tissue defect, but also in chronic wound care, plastic surgery, and congenital deformities."

**Conclusions:**

Sophisticated NMR and Mass Spectrometry instrumentation, supported by this award, links these four distinct defense-related projects. The consolidating hypothesis is that biomolecular structure and dynamics are key to the design of medical interventions

**Project 1 Mechanism of conversion of uridine to pseudouridine and to 4-thiouridine (Dr. E. G. Mueller).**

Professor Mueller's work has important implications in basic enzymology.

* The previously accepted mechanism of pseudouridine synthase TruA was shown to be incorrect. Instead of the expected product, the hydration product was demonstrated to be a dinucleodide. (McDonald et al, 2011)
* TruB, which handles the mechanistic probe 5-fluoroidine in RNA as a simple substrate rather than making a tight adduct (as Tru A does), converts 5-FU into two isomeric hydrated products that differ not in the hydrated pyrimidine ring but in the pentose ring, which is epimerized to arabinose in the minor product. This finding immediately suggested *a new mechanism* involving a glycal intermediate for the isomerization of uridine to pseudouridine. (Miracco and Mueller, 2011)
* The hydrated, rearranged product of 5-fluorodine, isolated as part of a dinucleoside, was found to undergo an unusual fragmentation during Mass spectrometry, with facile loss of HNCO from the product pyrimiding ring favored over phosphodiester bond rupture. Because the pericyclic process leading to this fragmentation cannot operate on a saturated pyrimidine ring, *a new mechanism was proposed*, which relies on the peculiar disposition of the functional groups of the product pyrimidine ring. (Miracco et al, 2011)

**Project 2. Devising new nanocomposites that can enhance wound healing (Dr. M. C. Yappert).**
In collaboration with Dr. Sufan Chien of the Department of Surgery, this project involves the delivery of ATP to wounded tissue. A proposal was submitted on July 11, 2012 to the Department of the Army. The potential impact of this work is listed below (as written in the technical abstract of the proposal. "This is the first time a non-traditional approach is used to treat massive soft tissue defects. The success of this technique will overturn current paradigm in massive soft tissue defect—no surgery (except hemostasis and debridement), no tissue engineering, no transplantation, and no sacrifice of healthy body parts are required. It will significantly improve soldiers' post-traumatic life, save billions of dollars in healthcare costs, and has the potential to open up a new avenue for tissue regeneration applicable not only in acute tissue defect, but also in chronic wound care, plastic surgery, and congenital deformities."

**Project 3 Characterization of the complex between Factor XIII and fibrinogen (Dr. M. C. Maurer).**
Thrombin, fibrinogen, and FXIII play critical roles in the last stages of blood coagulation. Thrombin is responsible for converting fibrinogen into fibrin which polymerizes into a soft clot. Activated FXIII then introduces covalent cross-links that help generate a rigid clot. These clotting proteins are being explored for medical applications that would of interest to the armed services and care of its personnel. Fibrinogen/fibrin has already been used as an attractive surgical sealant. In addition, biotechnology companies are currently researching better approaches for administering topical hemostatic agents. There are clear applications both in targeting wounds and in addressing surgical bleeding complications. Further research is needed to evaluate how fibrinogen, thrombin, and FXIII can be combined to create a more resilient clot. The current projects have provided valuable contributions toward achieving this goal. The fibrinogen αC 242-424 segment is an important binding region for enhancing activation of FXIII and also contains sites of reactivity within the fibrin clot. NMR and MALDI-TOF mass spectrometry approaches have been used to characterize structural features of this fibrinogen domain and its ability to serve as a FXIII substrate. For FXIII to serve as a therapeutic agent, more knowledge is needed on how to control FXIII activation. Kinetic and NMR studies have revealed FXIII mutants that are easier or more difficult to activate. Hydrogen-deuterium exchange coupled with MALDI-TOF mass spectrometry (HDX-MS) has indicated how FXIII $B_2$ can protect FXIII $A_2$ from premature activation and the role of calcium and sodium in regulating activation. Additional HDX-MS studies have revealed how thrombin can use exosite-active site and exosite-exosite interactions to promote conformational events that regulate thrombin function. Manipulating the characteristics of fibrinogen, thrombin, and FXIII shows much promise for designing clot architectures required for effective wound healing.

**Project 4. Tensile properties of fibrous proteins (Dr. R. J. Wittebort)**
We have developed new and novel $^2$H MQ methods devised that include several considerable improvements compared to the generally used methods for surface ordering studies. Inclusion of alignment and

purge significantly enhances S/N due to the detection of absorptive signal and therefore reduces the time required for the experiments. Spectra with excellent S/N can be obtained in experiments that last about one minute using small, single fiber samples. This allows us to perform experiments involving H/D exchange and single fiber samples which are ideal for evaluations of mechanical properties.

The approach for the design of the 2Q pulse sequence and phase cycles for MQ filtration that was successfully applied for $^{2}H$ can be adapted to any other quadrupolar nucleus. $^{17}O$ is particularly beneficial in aqueous solvent studies. Transition frequencies and basis operators for I=5/2 spins are provided in Appendix A. The large number of possible coherences and their interference make the development of the phase cycle for the selection of certain coherences the primary obstacle to overcome. New pulse sequences for $^{17}O$ studies will be required.

Comparisons between rubber and elastin for the amount of stretch induced changes in ordered solvent and the degree of ordering, clearly indicate important differences in their elastic mechanisms. The increase of the amount of ordered solvent with approximately constant quadrupolar coupling upon stretch are distinct from the results for rubber and indicate a significant role of the solvent in the elastic mechanism of elastin. Moreover, the increase in solvent ordering with increased temperature, demonstrates the importance of the hydrophobic effect in elastin recoil.

From this perspective, it will be interesting, to look at the variations in the amount of ordered solvent and strength of recoil when the hydrophobicity of the polymer is systematically varied. These studies are now in progress wherein designed elasrin-like sequences are prepared using recombinant protein methods. Analagous to proteins, we anticipate that in elastin the thermodynamic propensity for folding/recoil will increase if the protein's hydrophobicity is increased.

1. Weisel, J. W. (2005) Fibrinogen and fibrin. *Adv Protein Chem* **70**, 247-299
2. Ariens, R. A., Lai, T. S., Weisel, J. W., Greenberg, C. S., and Grant, P. J. (2002) Role of factor XIII in fibrin clot formation and effects of genetic polymorphisms. *Blood* **100**, 743-754
3. Lane, D. A., Philippou, H., and Huntington, J. A. (2005) Directing thrombin. *Blood* **106**, 2605-2612
4. Credo, R. B., Curtis, C. G., and Lorand, L. (1981) Alpha-chain domain of fibrinogen controls generation of fibrinoligase (coagulation factor XIIIa). Calcium ion regulatory aspects. *Biochemistry* **20**, 3770-3778
5. Smith, K. A., Adamson, P. J., Pease, R. J., Brown, J. M., Balmforth, A. J., Cordell, P. A., Ariens, R. A., Philippou, H., and Grant, P. J. (2010) Interactions between factor XIII and the alphaC region of fibrinogen. *Blood* **117**, 3460-3468
6. Shimba, N., Yamada, N., Yokoyama, K., and Suzuki, E. (2002) Enzymatic labeling of arbitrary proteins. *Anal Biochem* **301**, 123-127
7. Cleary, D. B., Doiphode, P. G., Sabo, T. M., and Maurer, M. C. (2009) A non-reactive glutamine residue of alpha2-antiplasmin promotes interactions with the factor XIII active site region. *J Thromb Haemost* **7**, 1947-1949
8. Karpati, L., Penke, B., Katona, E., Balogh, I., Vamosi, G., and Muszbek, L. (2000) A modified, optimized kinetic photometric assay for the determination of blood coagulation factor XIII activity in plasma. *Clin Chem* **46**, 1946-1955
9. Cleary, D. B., and Maurer, M. C. (2006) Characterizing the specificity of activated Factor XIII for glutamine-containing substrate peptides. *Biochim Biophys Acta* **1764**, 1207-1217
10. Isetti, G., and Maurer, M. C. (2004) Probing thrombin's ability to accommodate a V34F substitution within the factor XIII activation peptide segment (28-41). *J Pept Res* **63**, 241-252
11. Ariens, R. A., Philippou, H., Nagaswami, C., Weisel, J. W., Lane, D. A., and Grant, P. J. (2000) The factor XIII V34L polymorphism accelerates thrombin activation of factor XIII and affects cross-linked fibrin structure. *Blood* **96**, 988-995
12. Jadhav, M. A., Lucas, R. C., Goldsberry, W. N., and Maurer, M. C. (2011) Design of Factor XIII V34X activation peptides to control ability to interact with thrombin mutants. *Biochim Biophys Acta* **1814**, 1955-1963
13. Hoofnagle, A. N., Resing, K. A., and Ahn, N. G. (2003) Protein analysis by hydrogen exchange mass spectrometry. *Annu Rev Biophys Biomol Struct* **32**, 1-25
14. Muszbek, L., Bagoly, Z., Bereczky, Z., and Katona, E. (2008) The involvement of blood coagulation factor XIII in fibrinolysis and thrombosis. *Cardiovasc Hematol Agents Med Chem* **6**, 190-205
15. Woofter, R. T., and Maurer, M. C. (2011) Role of calcium in the conformational dynamics of factor XIII activation examined by hydrogen-deuterium exchange coupled with MALDI-TOF MS. *Arch Biochem Biophys* **512**, 87-95
16. Bock, P. E., Panizzi, P., and Verhamme, I. M. (2007) Exosites in the substrate specificity of blood coagulation reactions. *J Thromb Haemost* **5 Suppl 1**, 81-94
17. Naski, M. C., Lorand, L., and Shafer, J. A. (1991) Characterization of the kinetic pathway for fibrin promotion of alpha-thrombin-catalyzed activation of plasma factor XIII. *Biochemistry* **30**, 934-941
18. Sabo, T. M., and Maurer, M. C. (2009) Biophysical investigation of GpIbalpha binding to thrombin anion binding exosite II. *Biochemistry* **48**, 7110-7122

APPENDIX

## $^{17}$O MULTIPLE QUANTUM NMR

Task 4: d. Tensile properties of fibrous proteins (Dr. R. J. Wittebort)

$^{17}$O is potentially useful for characterization of weakly ordered water since it is not exchangeable with sites on the polymer, i.e. the signal originates only from the solvent. Moreover, the larger quadrupolar coupling implies more accurate determination of small order parameters, as in case of weakly ordered water. Implementation of MQ filtering approach to $^{17}$O requires more sophisticated than for $^{2}$H schemes for studying particular coherences. The pulse sequence and phase cycle devised in Chapter 3 for spins with $I=1$, require modification for $I=5/2$ ($^{17}$O) because the number of transitions is larger and additional actions are required to eliminate multiple quantum interference effects.

### A.1. Transition frequencies and operators

**Transition frequencies**

The transition frequencies at which different MQ coherences are evolving are calculated from the general formula

$$\omega^{mm'}=E^{m}-E^{m'}/\hbar,$$

for transition between states m and $m'$. Energy levels are

$$E^{m}=E^{m}_{os}+E^{m}_{q},$$

where $E^{m}_{os}$ and $E^{m}_{q}$ are the diagonal matrix elements

$$E^{m}_{os}=\langle m|H_{os}|m\rangle,$$

$$E^{m}_{q}=\langle m|H_{q}|m\rangle.$$

Hamiltonians $H_{os}$ and $H_{q}$ are given in chapter 3 (page 38). For $I=5/2$, possible spin states are m = 5/2, 3/2, 1/2, -1/2, -3/2, -5/2 and the quadrupolar coupling constant is $\omega_{q}=3eqQ^{2}/40\hbar$. To 1$^{st}$ order, only the part of $H_{q}$ that commutes with the Zeeman Hamiltonian, $H^{0}$, is required,

$$H_{q}=\omega_{q}\left(I_{z}^{2}-35/12\right).$$

In total, there are 15 possible transitions between 6 states as follows: 5 single quantum transitions (1Q), 4 double quantum transitions (2Q), 3 triple quantum transitions (3Q), 2 quadruple quantum transitions (4Q) and one pentuple quantum transition (5Q). The 1Q frequencies are

$$\omega_{12}=E^{-5/2}-E^{-3/2}=\Delta\omega_{os}+4\omega_{q},\ \omega_{23}=E^{-3/2}-E^{-1/2}=\Delta\omega_{os}+2\omega_{q},$$

$$\omega_{56}=E^{3/2}-E^{5/2}=\Delta\omega_{os}-4\omega_{q},\ \omega_{45}=E^{1/2}-E^{3/2}=\Delta\omega_{os}-2\omega_{q}\ \text{and}$$

$$\omega_{34}=E^{-5/2}-E^{-3/2}=\Delta\omega_{os},$$

with satellite splitting of 0, $4\omega_{q}$ and $8\omega_{q}$. 2Q frequencies are

$$\omega_{13}=E^{-5/2}-E^{-1/2}=2\Delta\omega_{os}+6\omega_{q},\ \omega_{24}=E^{-3/2}-E^{1/2}=2\Delta\omega_{os}+2\omega_{q},$$

$$\omega_{35}=E^{-1/2}-E^{3/2}=2\Delta\omega_{os}-6\omega_{q}\ \text{and}\ \omega_{46}=E^{1/2}-E^{5/2}=2\Delta\omega_{os}-2\omega_{q},$$

with satellite splitting $4\omega_{q}$ and $12\omega_{q}$. Three 3Q frequencies with satellite splitting 0 and $12\omega_{q}$ are

$$\omega_{14}=E^{-5/2}-E^{1/2}=3\Delta\omega_{os}+6\omega_{q},\ \omega_{25}=E^{-3/2}-E^{3/2}=3\Delta\omega_{os}\ \text{and}$$

$$\omega_{36}=E^{-1/2}-E^{5/2}=3\Delta\omega_{os}-6\omega_{q}.$$

The two 4Q transitions are

$\omega_{15} = E^{-5/2} - E^{3/2} = 4\Delta\omega_{os} + 4\omega_q$ and $\omega_{26} = E^{-3/2} - E^{5/2} = 4\Delta\omega_{os} - 4\omega_q$,
and a single 5Q transition frequency is
$\omega_{16} = E^{-5/2} - E^{5/2} = 5\Delta\omega_{os}$.
From above, it is clear that only two MQ coherencies are independent of the quadrupolar coupling. These are the 5Q and the central 3Q transition, which evolve at $5\Delta\omega_{os}$ and $3\Delta\omega_{os}$, respectively. Detection of these transitions is favorable since there is no quadrupolar broadening due to their independence on $\omega_q$.

**Basis operators**

For $^{17}$O, $I = 5/2$, there are $2I+1 = 6$ spin states and the density operator has $6 \times 6 = 36$ elements. Therefore, to represent the density operator as a linear combination of basis operators, the basis set has 36 operators. We use, as in the I = 1 case, a set obtained from single transition operators, $I_k^{rs}$. In addition to the identity operator, these are the coherences, $I_x^{rs}$ and $I_y^{rs}$ (for the 15 rs values), and 5 operators $I_z^{r,r+1}$ that are orthogonalized by the Gram-Schmidt procedure as follows:

$$O_z^{12} = I_z^{12}, \quad O_z^{23} = I_z^{23} - \frac{\mathrm{Tr}\left(O_z^{12} I_z^{23}\right)}{\mathrm{Tr}\left(O_z^{12} O_z^{12}\right)} O_z^{12},$$

$$O_z^{34} = I_z^{34} - \frac{\mathrm{Tr}\left(O_z^{23} I_z^{34}\right)}{\mathrm{Tr}\left(O_z^{23} O_z^{23}\right)} O_z^{23} - \frac{\mathrm{Tr}\left(O_z^{12} I_z^{34}\right)}{\mathrm{Tr}\left(O_z^{12} O_z^{12}\right)} O_z^{12},$$

$$O_z^{45} = I_z^{45} - \frac{\mathrm{Tr}\left(O_z^{34} I_z^{45}\right)}{\mathrm{Tr}\left(O_z^{34} O_z^{34}\right)} O_z^{34} - \frac{\mathrm{Tr}\left(O_z^{23} I_z^{45}\right)}{\mathrm{Tr}\left(O_z^{23} O_z^{23}\right)} O_z^{23} - \frac{\mathrm{Tr}\left(O_z^{12} I_z^{45}\right)}{\mathrm{Tr}\left(O_z^{12} O_z^{12}\right)} O_z^{12},$$

$$O_z^{56} = I_z^{56} - \frac{\mathrm{Tr}\left(O_z^{45} I_z^{56}\right)}{\mathrm{Tr}\left(O_z^{45} O_z^{45}\right)} O_z^{45} - \frac{\mathrm{Tr}\left(O_z^{34} I_z^{56}\right)}{\mathrm{Tr}\left(O_z^{34} O_z^{34}\right)} O_z^{34} - \frac{\mathrm{Tr}\left(O_z^{23} I_z^{56}\right)}{\mathrm{Tr}\left(O_z^{23} O_z^{23}\right)} O_z^{23} - \frac{\mathrm{Tr}\left(O_z^{12} I_z^{56}\right)}{\mathrm{Tr}\left(O_z^{12} O_z^{12}\right)} O_z^{12}.$$

Since $I_x^{rs}$ and $I_y^{rs}$ are normalized to $1/2$, $O_z^{r,r+1}$ are normalized also to $1/2$. These operators are given in Table A.1.

Table A.1. Matrix representations of orthogonalized operators for $I = 5/2$.

$$O_z^{12} = \begin{pmatrix} a & 0 & 0 & 0 & 0 & 0 \\ 0 & -a & 0 & 0 & 0 & 0 \\ 0 & 0 & 0 & 0 & 0 & 0 \\ 0 & 0 & 0 & 0 & 0 & 0 \\ 0 & 0 & 0 & 0 & 0 & 0 \\ 0 & 0 & 0 & 0 & 0 & 0 \end{pmatrix}, \; a = f(1) \qquad O_z^{23} = \begin{pmatrix} b & 0 & 0 & 0 & 0 & 0 \\ 0 & b & 0 & 0 & 0 & 0 \\ 0 & 0 & -2b & 0 & 0 & 0 \\ 0 & 0 & 0 & 0 & 0 & 0 \\ 0 & 0 & 0 & 0 & 0 & 0 \\ 0 & 0 & 0 & 0 & 0 & 0 \end{pmatrix}, \; b = f(2)$$

$$O_z^{34} = \begin{pmatrix} c & 0 & 0 & 0 & 0 & 0 \\ 0 & c & 0 & 0 & 0 & 0 \\ 0 & 0 & c & 0 & 0 & 0 \\ 0 & 0 & 0 & -3c & 0 & 0 \\ 0 & 0 & 0 & 0 & 0 & 0 \\ 0 & 0 & 0 & 0 & 0 & 0 \end{pmatrix}, \; c = f(3) \qquad O_z^{45} = \begin{pmatrix} d & 0 & 0 & 0 & 0 & 0 \\ 0 & d & 0 & 0 & 0 & 0 \\ 0 & 0 & d & 0 & 0 & 0 \\ 0 & 0 & 0 & d & 0 & 0 \\ 0 & 0 & 0 & 0 & -4d & 0 \\ 0 & 0 & 0 & 0 & 0 & 0 \end{pmatrix}, \; d = f(4)$$

$$O_z^{56} = \begin{pmatrix} e & 0 & 0 & 0 & 0 & 0 \\ 0 & e & 0 & 0 & 0 & 0 \\ 0 & 0 & e & 0 & 0 & 0 \\ 0 & 0 & 0 & e & 0 & 0 \\ 0 & 0 & 0 & 0 & e & 0 \\ 0 & 0 & 0 & 0 & 0 & -5e \end{pmatrix}, \; e = f(5) \qquad f(r) = \left[ 2r(r+1) \right]^{-1/2}$$

A.2. Scripts

Octave density matrix scripts allow numerical simulation of the evolution of the spin system during times and under the interactions determined by the pulse sequence. In addition, phases of the pulses are set separately and allow developing of a phase cycle. In this way, each coherence can be plotted as a function of preparation time and these graphs are used to determine optimal preparation times (maximum signal) for a given quadrupolar coupling. The "#" character indicates comment lines.

The script "mq_O17" simulates pulse sequence and phase cycle. An illustration of the settings used in the script is shown in Figure A.1. Main script "mq_O17" requires additional scripts for creation of relevant operators ("ops6levels"), simulation of RF pulses ("evol_ThPh") and evolution periods ("evol_Q_CS"). At any time current density operator can be decomposed into linear combination of basis operators using script "decomp".

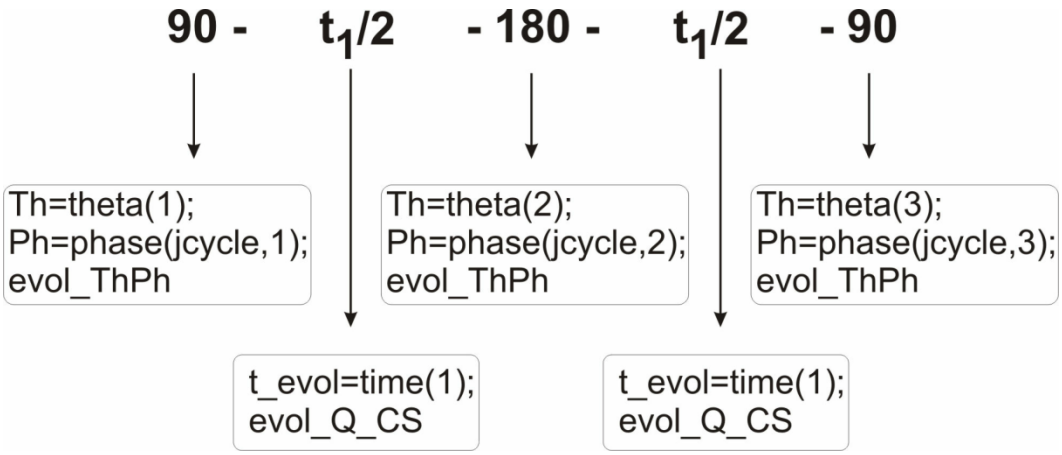


Figure A.1. Settings for the pulse sequence script, "mq_O17".

**mq_O17**

```
clear
I=5/2
# initiate the sequence by obtaining the necessary spin operators and by
# setting values of the quadrupolar coupling, vq, and offset (vos)
# frequencies (in Hz)
# delays
# 2*time(1) = evolution time in preparation and conversion, time(2)=echo delay
# for refocusing 2Q
# evolution, time(3)=2Q evolution following refocusing.
# Total time between 1Q to 2Q preparation and 2Q to 1Q conversion periods is
# 2*time(2)+time(3)
time=[.125,.10,0]

# pulses widths (deg) for all pulses
# in the order that they appear in the sequence
theta=[90,180,90,180,90,180]

# pulse phases phase(jcycle,kpulse) with jcycle=cycle number
# and kpulse=pulse number
phase= [0,90,90,0,90,0;
```

```
        0,180,90,0,90,0;
        0,0,90,90,0,0;
        0,0,90,90,90,0;
        90,0,180,90,0,0;
        0,0,90,0,90,0;
        0,0,0,270,0,0;
        0,0,0,315,0,0;
        180,180,180,0,0,0;
        180,180,180,45,0,0;
        180,180,180,90,0,0;
        180,180,180,135,0,0;
        180,180,180,180,0,0;
        180,180,180,225,0,0;
        180,180,180,270,0,0;
        180,180,180,315,0,0]

# set vos and vq
vq=1
vos=0
# Initialize sequence by creating relevant operators
ops6levels;
for jcycle=1:1:2;
# set the initial density operator to Iz
rho=Iz;
# step 1-5 of sequence, MQ preparation
Th=theta(1);
Ph=phase(jcycle,1);
evol_ThPh;
'coherences after initial 90'
decomp
t_evol=time(1);
evol_Q_CS;
Th=theta(2);
Ph=phase(jcycle,2);
evol_ThPh;
t_evol=time(1);
evol_Q_CS;
'coherences prior to 2nd 90 in preparation'
decomp
Th=theta(3);
Ph=phase(jcycle,3);
evol_ThPh;
'coherences after 2Q preparation is complete'
decomp

# steps 6-8, DQ echo and evolution
t_evol=time(2);
evol_Q_CS;
Th=theta(4);
Ph=phase(jcycle,4);
evol_ThPh;
t_evol=time(2);
evol_Q_CS;
'mq refocusing complete'
decomp
# MQ evolution following refocusing
```

```
t_evol=time(3);
evol_Q_CS;
'evolution complete, before conversion pulse'
decomp

# step 9 detection
Th=theta(5);
Ph=phase(jcycle,5);
evol_ThPh;
'coherences after conversion pulse'
decomp
endfor
```
**********

******

The script "ops6levels" creates basis operators for $I = 5/2$.

**ops6levels**

```
# Prepares the 30 6x6 matrix representations of spin 5/2 single transition
#coherences, Ix(r,s)=I(1,r,s,:,:) and Iy(2,r,s,:,:) ; r=1->5, s=r+1->6,
# 5 orthogonal polarization operators,I(3,r,s,:,:); r=1->5, s=r+1,
#Ix, Iy, Iz.
#and the raising and lowering operators, I+=Ip; I-=Im
dum=zeros(6);
for r=1:1:5;
        for s=r+1:1:6;
                I(1,r,s,:,:)=dum(:,:);
                I(1,r,s,r,s)=1/2;
                I(1,r,s,s,r)=1/2;
                I(2,r,s,:,:)=dum(:,:);
                I(2,r,s,r,s)=-i/2;
                I(2,r,s,s,r)=i/2;
        endfor;
endfor;
# check coherences
                for r=1:1:5
                        for s=r+1:1:6
                                r
                                s
                                x=dum;
                                x(:,:)=I(1,r,s,:,:)
                                y(:,:)=I(2,r,s,:,:)
                        endfor;
                endfor;
                x
                y
# create the 5 orthogonalized single quantum polarizations,
# I(2,r,s,:,:) r=1->5, s=r+1
for r=1:1:5
        s=r+1;
        I(3,r,s,:,:)=zeros(6);
endfor;
I(3,1,2,1,1)=1/2;
```

```
I(3,1,2,2,2)=-1/2;
a=sqrt(3/4);
I(3,2,3,1,1)=a/3;
I(3,2,3,2,2)=a/3;
I(3,2,3,3,3)=-2*a/3;
a=sqrt(2/3);
I(3,3,4,1,1)=a/4;
I(3,3,4,2,2)=a/4;
I(3,3,4,3,3)=a/4;
I(3,3,4,4,4)=-3*a/4;
a=sqrt(5/8);
I(3,4,5,1,1)=a/5;
I(3,4,5,2,2)=a/5;
I(3,4,5,3,3)=a/5;
I(3,4,5,4,4)=a/5;
I(3,4,5,5,5)=-4*a/5;
a=sqrt(3/5);
I(3,5,6,1,1)=a/6;
I(3,5,6,2,2)=a/6;
I(3,5,6,3,3)=a/6;
I(3,5,6,4,4)=a/6;
I(3,5,6,5,5)=a/6;
I(3,5,6,6,6)=-5*a/6;
# check polarization operators
for r=1:1:5
        r
        s=r+1
        z=dum;
        z(:,:)=I(3,r,s,:,:)
endfor
# check orthogonality
for j=1:1:5;
k=j+1;
        for j2=j+1:1:5;
        k2=j2+1;
        j
        k
        j2
        k2
        z1(:,:)=I(3,j,k,:,:);
        z2(:,:)=I(3,j2,k2,:,:);
        prod=trace(z1*z2)
        endfor
endfor
# set nuclear spin quantum number j (ex. j=5/2)
# matrix for the z-component of angular momentum
# general case of spin j, Hilbert space has 2j+1 dimensions
Iz
j=5/2;
Iz=diag([j:-1:-j]);
# matrix for the x-component of angular momentum
Ix
Ix=zeros(2*j+1);
n=1;
while (n<2*j+1)
Ix(n,n+1)=0.5*sqrt(n*(2*j+1-n));
```

```
Ix(n+1,n)=0.5*sqrt(n*(2*j+1-n));
n++;
endwhile
Ix
# matrix for the y-component of angular momentum
# Iz and Ix are defined, so we just use commutator [IzIx]=iIy to find Iy
Iy=(1/i)*(Iz*Ix-Ix*Iz);
ck=i*(Iy*Ix-Ix*Iy)
Ip=Ix+i*Iy
```

**********

******

The script “evol_ThPh” calculates the effect of an RF pulse with flip angle Th and phase Ph on the current density operator, rho.

**evol_ThPh**

```
# evolution of the current density operator, rho, subject to a hard RF
# pulse with flip angle Th (deg) and phase Ph (deg)
phir=pi*Ph/180;
thetar=pi*Th/180;
op=(cos(phir)*Ix)+(sin(phir)*Iy);
prop=expm(-i*(thetar)*op);
r=prop'*rho*prop;
rho=r
```

**********

******

The script “evol_Q_CS” calculates the effect of evolution under quadrupolar coupling and chemical shift on the current density operator, rho.

**evol_Q_CS**

```
wq=2*pi*vq;
wos=2*pi*vos;
Id=((sp*(sp+1))/3)*eye(2*sp+1);
Hq=wq*((Iz*Iz)-Id);
Hcs=wos*Iz;
dum=i*(Hcs+Hq)*t_evol;
prop=expm(-dum);
r=prop'*rho*prop;
rho=r
```

**********

******

The script “decomp” takes the current density operator, rho, and decomposes it into a linear combination of basis operators.

**decomp**

```
# decompose the density operator, rho, into single transition operators
```

```
# and store in the complex vector st(q). For elements q=1-->15, real(st) and
# imag(st) are Ix(rs), Iy(rs), respectively, in the order (r,s) = (1,2), (1,3),.....(1,6),
# (2,3)...(5,6). Orthogonalized Iz(r,s) coefficients (real) are q=16-->20 in the order
# (r,s) = (1,2), (2,3).....(5,6). Finally, coefficients for Ix and Iy are real(st(21) and
# imag(st(21)), i.e., st(21)=trace(I+*rho), and Iz=s(22).
q=0;
for r=1:1:5;
        for s=r+1:1:6;
                q=q+1;
                dum=2*real(rho(r,s));
                st(q)=dum;
                dum=-2*imag(rho(r,s));
                st(q)=st(q)+i*dum;
        endfor;
endfor;
l=15;
for r=1:1:5;
s=r+1;
l=l+1;
        dum=0;
        for jk=1,6;
                dum=dum+(I(3,r,s,jk,jk)*rho(jk,jk));
        endfor;
        st(l)=dum;
endfor
st(21)=trace(Ip*rho);
st(22)=trace(Iz*rho);
v1q=[st(1),st(6),st(10),st(13),st(15)]
v2q=[st(2),st(7),st(11),st(14)]
v3q=[st(3),st(8),st(12)]
v4q=[st(4),st(9)]
v5q=[st(5)]
*********************************************************************************************

******
```